מכון ויצמן למדע

Weizmann Institute of Science

Thesis for the degree of
Doctor of philosophy

חיבור לשם קבלת התואר
דוקטור לפילוסופיה

By
Yossi Yayon

מאת
יוסי יאיון

אפיון אי-הסדר בבור קוואנטי על ידי מיקרוסקופ אופטי שדה קרוב

Characterization of the Disorder in a GaAs Quantum Well by Near-Field Optical Spectroscopy.

Supervisor: Prof. Israel Bar-Joseph

מנחה: פרופ' ישראל בר-יוסף

May 2003

אייר תשס"א

Submitted to the Scientific Council of the
Weizmann Institute of Science
Rehovot, Israel.

מוגש למועצה המדעית של
מכון ויצמן למדע
רחובות, ישראל

ProQuest LLC
789 East Eisenhower Parkway
P.O. Box 1346
Ann Arbor, MI 48106-1346

Acknowledgments

I wish to thank all those who helped me reach this goal.

In particular, I am grateful to Israel Bar-Joseph, my supervisor for the last eight years, for always providing assistance, encouragement and a good advice (not only in physics).

I'm glad to thank Michael Rappaport for his extremely useful assistance in this research work and friendly support in a variety of technical matters and for being a great company in two conferences.

Thanks to all the students in our group, Javier Groshaus, Erel Morris, Tali Dadosh and Yoav Gordin for their assistance, and useful discussions.

I thank Vadim Shofman for helping in the fabrication of the SNOM tips.

I thank all the students in the Sub-Micron center for the good atmosphere in the center and for their useful help.

I thank all the staff members of the center for their contribution to this research work, and in particular, Vladimir Umansky, Hadas Shtrikman and Sharon Waschitz for growing MBE samples, Diana Mahalu for the E-beam writing, Olga Raslin for her assistance with the evaporators, and Yoram Rotblat and Yossi Rolnik for their technical support.

I would like to thank Yossi Gal, Solomon Shpiner, and Ronen Havkin for their quick response to my helium orders and for taking care of my fish aquarium while I'm away.

Abstract

The two-dimensional electron system (2DES) formed in a semiconductor quantum well (QW) has been a major experimental system in condensed matter physics for the last few decades. It plays an important role both in the investigation of the physics of two-dimensional systems and in microelectronics and electro-optics applications. Disorder in the QW structure and in the 2DES density distribution was found to have a major effect on many transport and optical phenomena, which are observed in this system: the integer and fractional quantum Hall effects, the metal insulator transition, anisotropy current distribution, resonant Rayleigh scattering, electrons and excitons localization, condensation of excitons and more.

In this work I performed local optical spectroscopy measurements of 2DES in a QW in order to characterize its disorder and to understand its implications on its macroscopic properties. I developed and built a low temperature scanning near-field optical microscope. Using this microscope I measured the local photoluminescence (PL) spectrum and analyzed the distribution of various parameters, such as peak energies, peak intensities and line shapes. From these measurements I extract information on the local electron density, well width, electrostatic potential and background doping, and to understand the far-field PL spectrum.

Three disorder mechanisms are studied:

- *Inhomogeneity in the MBE growth process*, which gives rise to fluctuations in the thickness of various layers, and in particular – the QW width and spacer thickness. We find surprising long-range correlations in the well-width fluctuations and in the electron density distribution in the QW plane. The electrons are arranged in stripes elongated parallel to the $[1\bar{1}0]$ crystallographic direction and the well-width fluctuations create a cubic like structure. We associate these correlations with the known mounds formation process during MBE growth. We also find a strong correlation between the width fluctuations of different wells grown one on top of the other.
- *The donors random distribution*, which creates a fluctuating electrostatic potential at the 2DES plane. This electrostatic potential localizes the electrons in the QW plane. We find a new broadening mechanism of the exciton, where electron

density fluctuations give rise to a significant inhomogeneous broadening of the exciton peak. On the other hand the negatively charged exciton peak is homogenously broadened. We introduce a novel method to extract the electron density from charged exciton line.

- *The GaAs background doping*, which is a major electron scattering mechanism. To identify the local position and binding energies of the background acceptors in the QW we perform near-field PL measurements in a high magnetic field. The acceptors are marked by a low-energy replica of the 2DES spectrum.

Introduction

In the first two sections of the introduction (1.1-1.2) I'll give a brief theoretical and experimental description of the near-field microscope system. In the rest of the introduction (1.3-1.5) I'll discuss a few issues related to the physics of disordered 2DES and closely connected to my work.

1.1 Near-field microscopy

The scanning near-field optical microscope (SNOM) was invented in 1984 [1], and since then it is used in many fields of physics where a sub-wavelength optical resolution is required. It belongs to a wide family of scanning probe microscopes which includes the scanning tunneling microscope (STM) [2], the atomic force microscope (AFM) [3] and many others. In a SNOM the tip that scans the sample is a tapered optical fiber which collects/transmits light through a sub-wavelength aperture.

In the next two subsections I'll give a brief theoretical review of the resolution limit of classical optics and how it is overcome by near-field optics.

1.1.1 Classical Imaging

Let us begin with a brief description of the classical imaging theory and its resolution limit. In Fig. 1 we consider a general imaging system, and we presume that it has an entrance and an exit apertures. In the far field approximation it is assumed that the passage of light between the entrance and exit planes can be described in terms of geometric optics. Thus, the entrance and exit apertures are effectively the geometrical projection of each other [4].

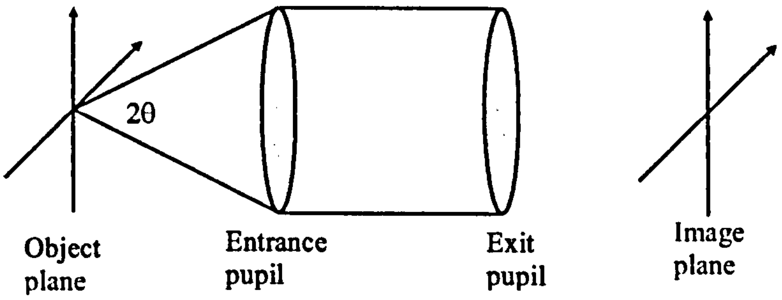

Fig. 1: General model of an imaging system.

Let us first consider a line source, located at the object plane. The light intensity of a line source at x=x$_0$ is described by: $f(x)=\delta(x-x_0)$. The angular spectrum of such a source is:

$$f(k)=\int_{-\infty}^{\infty}\delta(x-x_0)e^{ikx}dx=e^{ikx_0}.$$

When this object is imaged with an imaging system, whose objective accepts an aperture angle of 2θ, only spatial frequencies $|k_x|$ in the range $[0,k_{\max}=\omega n\sin(\theta)/c]$ are admitted by the apparatus, where ω is the light frequency and n is the refractive index of the medium between the object and the entrance pupil. The image that can be constructed, at the image plane, is given by:

$$f(x)=\int_{-k_{\max}}^{k_{\max}}e^{ikx_0}e^{-ikx}dk=\frac{2\sin[\omega n\sin(\theta)(x-x_0)/c]}{x-x_0}.$$

Although the source is infinitely narrow, it is seen at the image plane as a light line with a finite width. The first zero of the sinc function is at

$$x-x_0=\frac{\pi c}{\omega n\sin(\theta)}=\frac{\lambda}{2n\sin(\theta)}.$$

When having two line sources, the resolution given by the Rayleigh criterion (the minimum of one source is at the maximum of the second source) is:

$$\Delta x=\frac{\lambda}{2n\sin(\theta)}.$$

In the case of a point source and a circular aperture, the image will be an Airy disc. The resolution, which is then given by the width of the Airy disc function, is [5]

$$\Delta x=\frac{0.61\lambda}{n\sin(\theta)}.$$

To go beyond this resolution limit, the imaging device should be able to collect higher spatial frequencies than $k_x={}^{\omega n}\!/_{c}$. This is done by the SNOM.

1.1.2 Near-field optics

As I have shown above, it is commonly accepted that the resolution limit of an imaging system is of the order of the light wavelength. This is true if the optical aperture is positioned at least a few wavelengths from the object and the aperture size is larger than the wavelength. These conditions are normally fulfilled in practice so they are usually ignored.

It is easy to understand the origin of these conditions using an analysis based on Fourier optics [6]. Consider a monochromatic optical field, E(x,z), propagating in the z direction, and its angular spectrum, E(k_x,z). They relate as:

$$E(x,z)=\int_{-\infty}^{\infty}E(k_x,z)e^{-ik_x x}dk_x\,.$$

Since E(x,z) must satisfy the wave equation, the spectral amplitudes are known to satisfy the propagation relation :

$$E(k_x,z)=E(k_x,0)e^{ik_z z},$$

and since

$$k^2=k_x^2+k_z^2=\left(\omega/c\right)^2,$$

we get

$$E(k_x,z)=E(k_x,0)e^{i\sqrt{k^2-k_x^2}\,z},$$

where I assumed n=1.

If the field has spectral amplitudes, E(k_x,z), which are different from zero, for $k_x>\omega/c$, they will be evanescent, decreasing exponentially with increasing z. The low frequency components ($k_x<\omega/c$) do not damp out but propagate as plane waves, traveling at angles $\theta=\sin^{-1}(k_x\lambda/2\pi)$. The high frequency components ($k_x>\omega/c$) have significant contribution only when $z<<\lambda$, so in order to achieve a resolution better than λ the aperture of the optical system must be much closer than λ to the measured object.

It is not enough to place the aperture close to the object. The imaging system should also have the ability to convert those evanescent waves into propagating waves, which will be seen far from the object. It follows from the theory of diffraction that a small object, illuminated with a propagating wave, generates diffracted evanescent waves. By applying the reciprocity theorem we find that a small object located in an evanescent field converts part of this field into propagating waves [7,8]. Therefore, in order to detect the evanescent waves, that contain information about the small details of the object, one has to use a diffraction center of sub-wavelength size (the tip), and locate it at a sub-wavelength distance from the surface to be explored.

1.2 Instrumentation

In this work I was interested in performing local spatial spectroscopy measurements of the photoluminescence emitted from GaAs quantum wells. The relevant spatial resolution of the processes in a quantum well is much smaller than the photoluminescence wavelength (~800 nm). As I explained previously this excludes the use of far-field imaging systems for such measurements, which have a spatial resolution limit of the order of the light wavelength (see introduction).

The operation principle of our SNOM is very simple. By approaching a sub-wavelength aperture (the fiber tip) to the close proximity of the sample, the evanescent waves from a small area are collected by the tip and transformed into propagating ones. By scanning the tip over the sample, an image with a sub-wavelength resolution is obtained.

To be able to perform spectroscopic measurement of GaAs QWs with high spatial resolution we developed and built a SNOM. The system we built has the following specifications which are not available commercially in one system.

1. It works at low temperature ($\leq$ 4.2 K).
2. Unlike most SNOM systems that work in illumination mode, (the fiber tip illuminates and excites the sample) it operates in collection mode, where the fiber tip collects the PL emitted from the sample. This mode provides higher spatial resolution and low excitation of the sample.
3. Since the GaAs substrate is opaque the illumination and collection of the light are done at the same side of the sample (in common SNOMs they are on opposite sides of the sample, since it simplifies the design).
4. It is compact enough (diameter ~ 33 mm) to be inserted into the bore of a superconductor magnet.
5. It collects the PL with high efficiency. This is of importance since the emitted signal from a single QW is very weak. For that we fabricated high transmission efficiency tips by using the tube etching method and coating by a thin film of metal.

6. The tip-sample distance regulation is based on a non-optical method, since the Helium Dewar and the magnet are opaque to the laser light. We used a method based on a quartz tuning fork.

The design and operation of our SNOM are described in paper # 1. Here I would like to discuss in more details two important issues of all SNOM systems.

1.2.1 Tip-sample distance regulation

Common distance control methods are based on optical detection of shear force acting on the tip. In such a detection method, the tip is usually vibrated in a direction parallel to the sample surface at one of its mechanical resonances. As it approaches a distance of a few tens of nanometers above the sample surface, the amplitude of the tip vibration decreases. This damping of the vibration amplitude is due to the tip-sample interaction. Optical detection of the tip vibration amplitude can be performed by measuring the oscillations in the reflected intensity of a laser beam focused on the tip end [9,10]. In our SNOM it is difficult to implement this method, because we are interested in measurements at low temperatures, and in a magnetic field. One therefore has to use non-optical distance regulation methods. Such methods have been proposed and demonstrated. Some are based on attaching the tip to a piezoelectric tube and detecting the tip resonance amplitude in the piezoelectric signal [11,12]. Others detect the tip resonance amplitude and phase directly by attaching it to a tuning fork [13,14].

In the present design, we take advantage of the mechanical resonance of a piezoelectric tuning fork with a large quality factor [15]. As shown in Fig. 2, the optical fiber with its aluminized tapered tip is glued along the side of one of the prongs of a quarts crystal tuning fork. Such tuning forks are commercially available for operation at 32768 Hz. In order to excite the mechanical resonance of the fork, it is rigidly mounted on a ceramic piezoelectric tube serving as a dither. The tuning fork and the tip are vibrated parallel to the sample surface. On resonance, the bending amplitude of the prongs is maximal. This bending of the prongs generates an oscillating piezoelectric potential on the fork electrodes, which are proportional to the tip oscillation amplitude. Hence, by measuring this voltage one gets a signal which is directly related to the prongs bending.

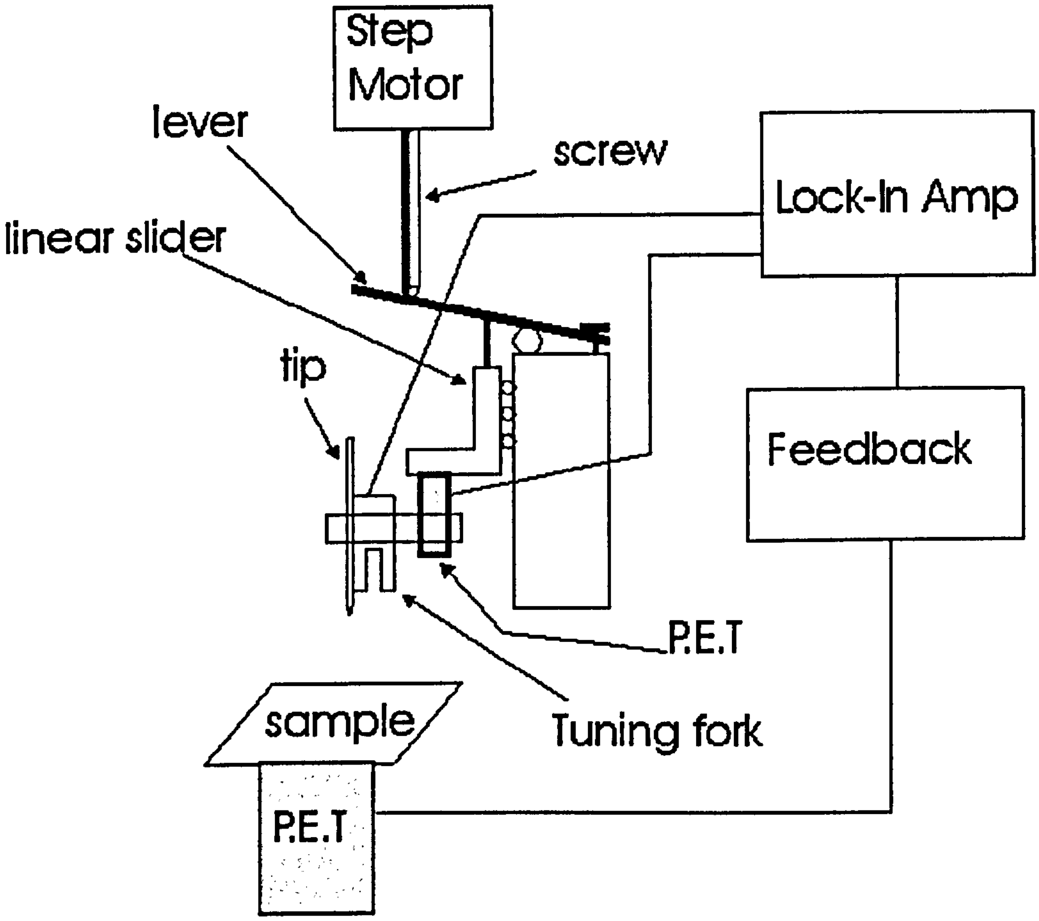

Fig. 2: A diagram of the tip-sample distance regulation system.

It is important to apply a low drag force on the tip to prevent damage to it. The amplitude of the drag force is given by:

$$|F_D| = F = \frac{kA_0}{\sqrt{3}Q}.$$

The tip amplitude, A_0, is determined from the electric signal of the fork, according to the calibration of 27 μV/nm at room temperature, and about one tenth of it at 4.2 K. The resonance quality factor, Q, is found from the resonance curve (Fig. 3). k is the static compliance of one prong and is calculated from the fork geometrical dimensions. A typical drag force, acting on the tip in our system, is a few tens of nN.

Typical curves describing the piezoelectric signal amplitude as a function of frequency are shown in Fig. 3. The solid line is measured with a free fork at room temperature, the dashed line is measured with a fork that a tip is attached to it, also at room temperature, and the dotted line is the same as the dashed line, but at a low temperature (4.2 K). The free fork amplitude is divided by 4, and the low temperature amplitude is multiplied by 3 for viewing convenience. One can see that there is a significant reduction of the quality factor and shift of the resonance frequency after attaching the tip to the tuning fork. When cooling the SNOM the resonance narrows and shifts to higher frequency.

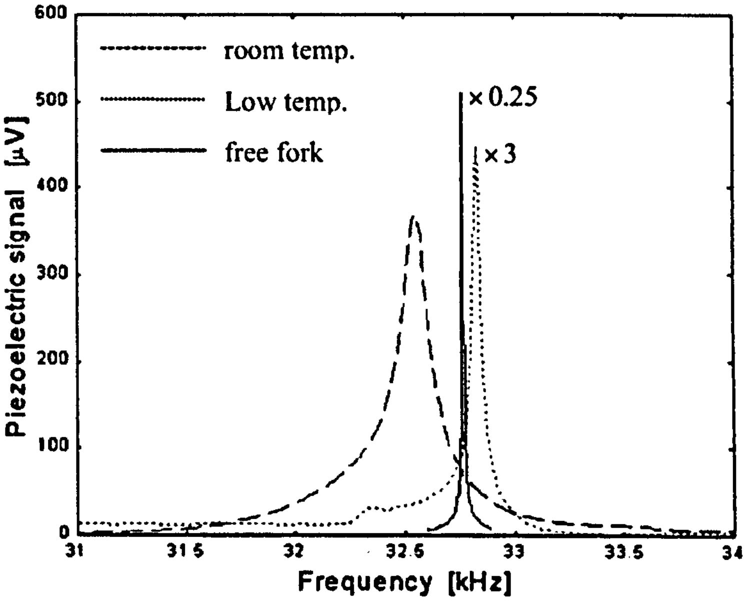

Fig. 3: The Amplitude of the piezoelectric signal as a function of the driving frequency. The dither piezoelectric tube is driven with a signal of 100 mV. The solid line is measured with a free fork, the dashed line is measured with a fork which has a tip attached to it at room temperature, and the dotted line is the same as the dashed line, but at low temperature (4.2 K degrees).

When used for feedback, the fork is driven at resonance. The oscillating signal, picked up between the two contacts of the tuning fork and measured using a lock-in amplifier synchronized with the dither frequency, is monitored by the feedback system as the tip approaches the sample. A reduction in the amplitude of that signal is measured when the tip is within ~20 nm of the sample surface. This change in the signal is shown in Fig. 4.

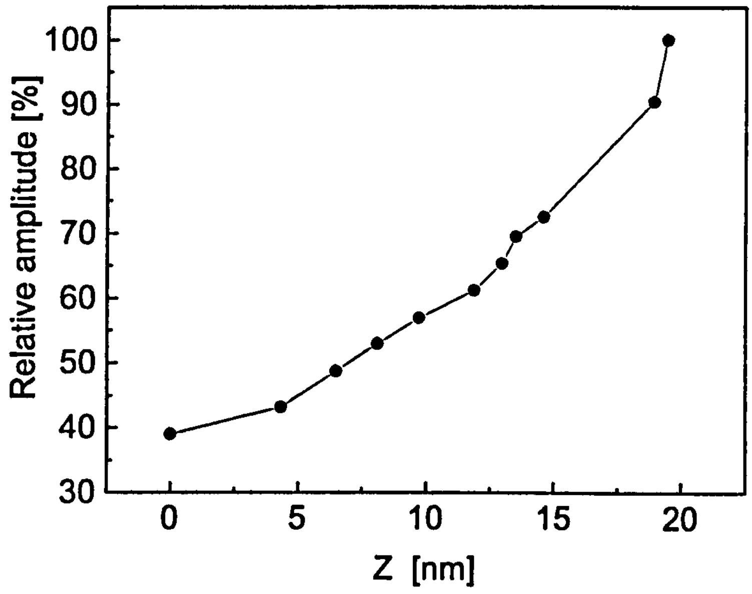

Fig. 4 : Approach curve of the normalized signal amplitude as a function of the tip-sample distance. The measurement has been made at a temperature of 4.2 K.

Such piezoelectric signals can be used in conjunction with an electronic feedback loop for keeping the tip at a constant distance from the sample surface (~ 5-20 nm). If this signal is smaller/higher than a pre-determined set-point of the feedback system, then the piezoelectric tube, to which the sample is attached, shrinks/stretches until the signal is equal to the set-point, and the tip is brought to the correct distance from the sample.

The signal of the voltage applied to the piezoelectric tube can be used for surface topography imaging, as demonstrated in Fig. 5. In this example the topography was fabricated by etching of GaAs mesa lines. The depth of the etching is 300 nm, the width of the lines is 6 μm and the period is 10 μm. The structure was scanned, perpendicular to the mesa lines (in the Y direction), in steps of 100 nm. The noise in the topography measurement is manifested in the small roughness of the top of the mesa lines. We can see that the etched areas exhibit significantly larger roughness compared with the non-etched areas. This is a true effect, resulting from the inhomogeneity of the etching.

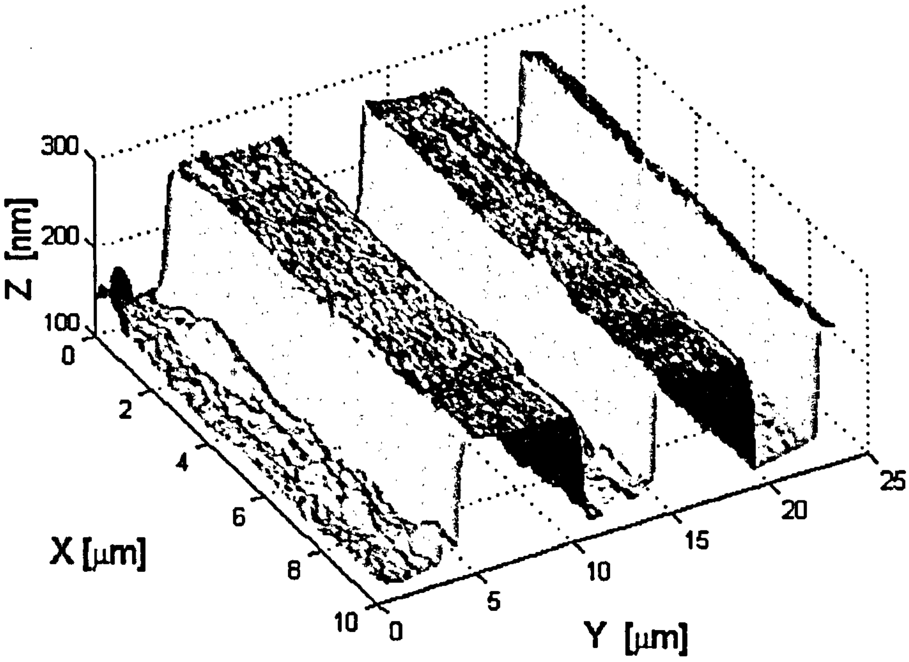

Fig. 5: A scan of etched mesa lines. The width of the lines is 6 μm and the period is 10 μm. The surface was scanned perpendicular to the lines direction (in the Y direction). The step size is 100 nm.

1.2.2 Tip fabrication

The fiber tip plays a major role in all SNOMs. The desired tip is one with a small aperture and large transmission. Several tip preparation techniques have been reported in the literature, including mechanical pulling [16-23], chemical etching [24-30], and a combination of both of them. The method we decided to use is based on tube etching of an optical fiber in hydrofluoric acid covered with an organic oil layer [31,32]. With this method it is possible to obtain tips with a large cone angle, a smooth surface and an aperture diameter of less than 100 nm.

This method is schematically demonstrated in Fig. 6. The HF solution diffuses through the fiber jacket and etches the fiber. The flow direction creates a smooth cone shape at the end of the fiber. The resulting tip shape depends on many parameters of the etching process such as the acid temperature and concentration, length of fiber inserted into the acid, and time of etching. We varied these parameters to obtain the tip desired for our purpose.

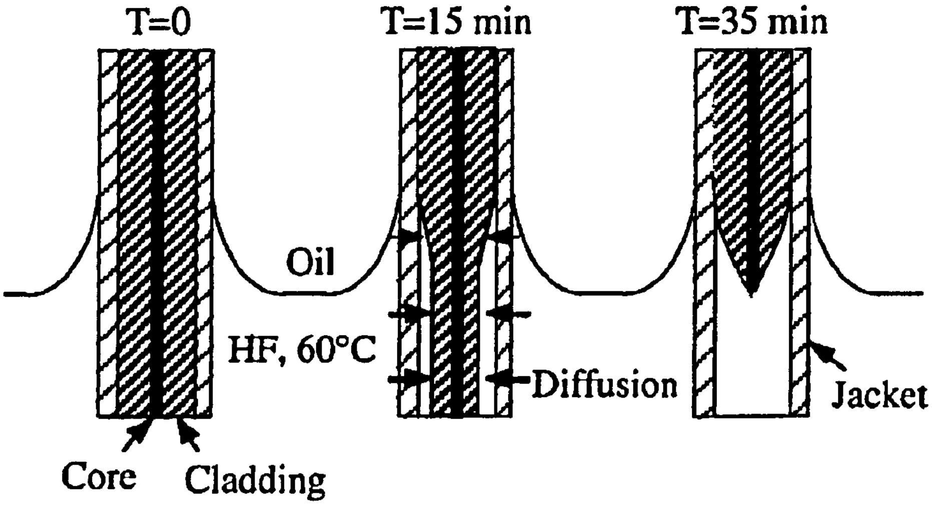

Fig. 6: Taken from reference 31. An optical fiber is dipped, with its acrylate jacket, in aqueous hydrofluorydic acid covered by oil as a protective layer. The acid diffuses through the acrylate and etches the quarts fiber. After 35 min a sharp tip is formed.

A scanning Electron Microscope (SEM) picture of a fiber tip, which was pulled out from the etching acid, before the end of the process (after 50 min) is shown in Fig. 7 (a). One can see the formation of the cone as well as the narrow and long part, as schematically shown in Fig. 6. By etching longer the narrow part is etched away and a smooth cone is left (Fig. 7 (b) and (c)). The cone angle calculated from the figure is $\sim 30^{\circ}$. We succeeded in getting cone angles up to 50°. Typically the aperture diameter (the flat area at the end of the tip) obtained in this process is smaller than 50 nm. We are interested in larger apertures to increase the light transmission of the tip. To reach this goal we raise the level of the acid, after the etching process is done, by inserting a small object into the etching solution. Thus, the end part of the tip is etched away and a flat aperture with the desired diameter is obtained (see Fig. 7 (c)).

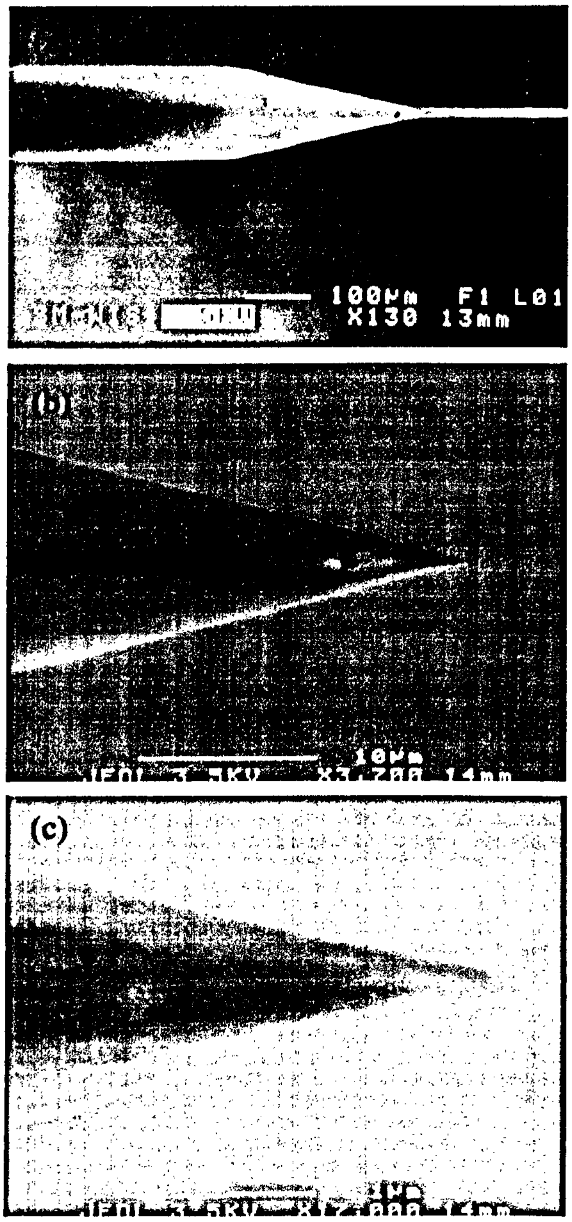

Fig. 7: (a) A SEM image of a fiber tip after 50 min in the etching liquid. (b) and (c) SEM images of an etched fiber tip at two different magnifications.

After the etching we evaporate metal on the fiber to define the aperture for the light at the end of the tip. We use a thin layer of Chromium (~5 nm) for improving the adhesion and on top of it a layer of gold (~200 nm). A tip after the evaporation is seen in Fig. 8.

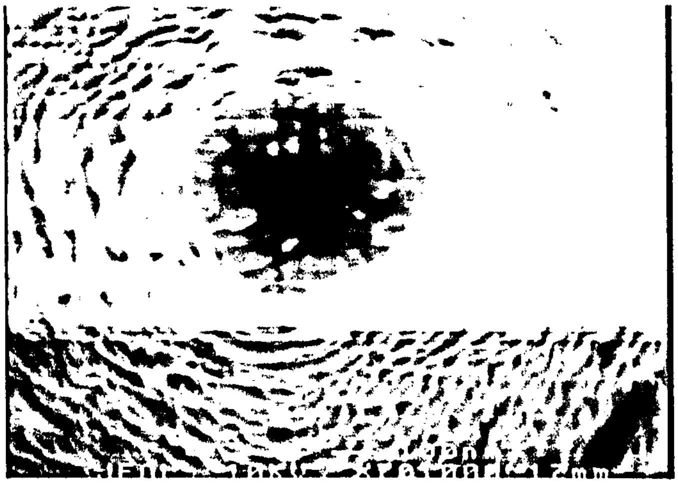

Fig. 8: A fiber tip after evaporation of gold.

Using this process we obtained tips with high transmission of the order of 10^{-2} at a diameter of 200 nm. We also checked their damage power (the maximum intensity that can be transmitted), and were able to get out of the tip $30\mu W$ without damaging the tip coating.

One of the difficulties that still should be solved is fabricating tips that are circularly symmetric. It seems that in this fabrication method the resulting tips have some anisotropy due to inhomogeneous flow of the HF acid. This should be important when performing polarized near-field measurements.

The design and operation of the SNOM are described in the following paper:

- G. Eytan, Y. Yayon, I. Bar-Joseph, and M. L. Rappaport, "A storage Dewar near-field scanning optical microscope", Ultramicroscopy, **83**, 25 (2000).

1.3 Two dimensional electron system in a quantum well

In the next three subsections I shall describe general aspects of a 2DES which are important for the understanding of my work. First I shall outline the structure of a typical sample I used: a gated 2DES in a QW. Then I introduce three disorder mechanisms which I measured and characterized during my research. In the last part I give a brief introduction to the behavior of 2DES in a perpendicular magnetic field which is helpful for understanding the section dealing with the mapping of the background doping (section 2.2).

1.3.1 Typical structure

The samples I used are QWs formed by GaAs/AlGaAs double heterostructures (see Fig. 9) grown by the molecular beam epitaxy (MBE) technique. It is formed by growing a layer of low band gap material (GaAs) embedded between two layers of high band gap material (AlGaAs). The electrons in the QW come from a remote donors (Si atoms) layer. High mobility 2DES is achieved by separating the donors layer from the QW with a spacer layer of typical width of ~ 50-100 nm. On top of the sample we evaporate a semitransparent gate (5 nm of PdAu) and create contacts to the gate and 2DES. By applying a voltage between the gate and the QW we control the 2DES average density. All the measurements were done at a temperature of 4.2 K.

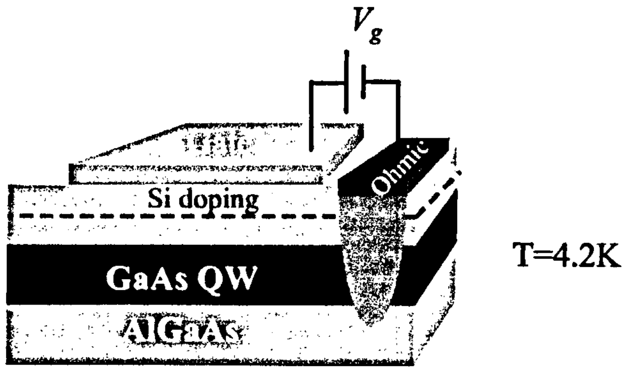

Fig. 9: A schematic drawing of a typical gated 2DES structure.

1.3.2 Disorder

When we use the term disorder we refer to any inhomogeneity in the sample which affects its optical or electrical properties. In this work I discuss three main disorder mechanisms in a QW:

- **Inhomogeneity in the MBE growth process:** A layer, grown by the MBE technique, is not atomically flat and has some width fluctuations due to imperfection of the growth process and to intrinsic growth instability of the last grown monolayer in the presence of the so-called Ehrlich-Schwoebel diffusion barriers [33,34]. These fluctuations contribute to two disorder effects. The first is electron energy fluctuations. The quantization energy, E, of the charge carriers in the well depends on the well width. For infinite barriers well, the fluctuations in the energy, ΔE, are related to the well width fluctuations by the relation: $\Delta E/E = -2\Delta W/W$ where W and ΔW are the well width and its fluctuations, respectively. For a well of 20 nm, a fluctuation of one monolayer (0.28 nm) results in $|\Delta E| \sim 0.2meV$. The second disorder effect is electron density fluctuations due to variations in the distance between the QW and a constant potential layer (surface, gate, uniform donors layer). If we think about the system as a parallel plate capacitor then width fluctuations are manifested as variations in the distance between the two plates and hence will create density fluctuations in the 2DES. These two effects will be quantitatively analyzed in 1.5.1 and 1.5.2.
- **Donors random distribution:** The ionized donors are randomly distributed in the plane and hence they create a random electrostatic potential in the 2DES plane. If we denote the donors average two-dimensional density as n_d and the distance between the 2DES and the donors plane as s then the average charge fluctuation of spatial wavelength $R > s$ is $e\sqrt{n_d R^2}$. This will generate potential fluctuations of the order $\sim e^2\sqrt{n_d}/\varepsilon$ for $R > s$ [35-37]. The 2DES is arranged in the plane in such a way that it screens these potential fluctuations.

- **Background doping:** In practice an intrinsic semiconductor is not ideally pure and it contains some density of impurity atoms. In our MBE system a typical density of the background impurities is $\sim 10^{14} - 10^{15} cm^{-3}$ and they behave as acceptors. They can capture and release an electron from the 2DES and hence affect its optical and transport properties.

1.3.3 2DES in a perpendicular magnetic field

Although I won't discuss in my thesis the work I have done that concerns the physics of 2DES in a magnetic field, I will describe here only a few basic aspects of it which will be helpful in chapter 2.2 in identifying the spatial position and binding energy of the background acceptors.

When a magnetic field is applied perpendicular to a 2DES, the electron energy spectrum is transformed into a discrete spectrum of Landau levels (LLs). It consists of equally spaced energy levels, $E_n = (n + 1/2)\hbar\omega_c$, where $\omega_c = eB/m$ is the cyclotron frequency. Each of these levels splits into two with the energy difference between them being the Zeeman energy, $E_Z = g\mu_B B$. The degeneracy of each level is $N_{LL} = \frac{2eBA}{h}$, where A is the area of the sample and the number of filled levels (filling factor) is $\nu = \frac{h}{2eB} n_e$, where n_e is the 2DES density.

The magnetic field has a clear and unique signature on the PL spectrum. In Fig. 10 a typical PL measurements in a varying magnetic field is presented. Each PL spectrum (horizontal cut of the figure) consists of (approximately) equally spaced peaks which correspond to the different LLs (each peak corresponds to the two spin levels which are not resolved in this measurement). A certain LL is seen in the spectrum when it is occupied and its intensity vanishes when it empties. Thus, the even ν's are seen as abrupt disappearance of a certain LL from the spectrum. It can be seen that the LLs energy depends linearly on the magnetic field and that the filling factor decreases with increasing the magnetic field.

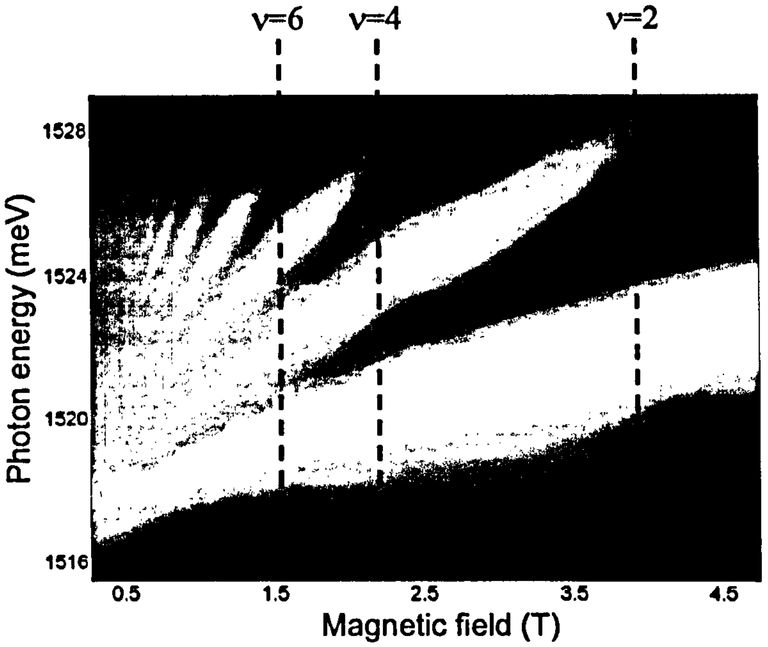

Fig. 10: Grayscale color-coded map of a PL measurement in a magnetic field. Bright colors represent high intensity.

1.4 Excitonic spectrum in the presence of a two-dimensional electron system

The PL spectrum of a low density 2DES has been the subject of considerable interest in recent years. It is observed that at a certain critical density, which depends on sample parameters, but is typically between $10^{10}-10^{11}cm^{-2}$, the spectrum abruptly changes from a broad line at high densities to two narrow peaks at low densities. A number of spectroscopy experiments at zero and high magnetic fields have clearly shown that the two peaks are associated with the neutral exciton (X) and negatively charged exciton (X^-) [38-40]. The X is a bound state of a photoexcited electron-hole pair and the

X^- is formed by the binding of a photoexcited electron-hole pair to an electron from the 2DES.

1.4.1 Extracting the electron density from the PL spectrum

It has been realized already at the earliest observations of the X –X^- spectrum that the strength of each of these PL lines is related to the background electron density: it was observed that as the density is lowered the X intensity diminishes, and the spectrum becomes dominated by the X line (see Fig. 11). It has also been noticed that the X and X^- lineshapes are different: while the X lineshape fits well a Gaussian function, the X^- one fits more a Lorentzian function [41]. Nevertheless, there is no quantitative theory that reliably relates the observed spectrum and the 2DES properties.

In this work I present a method to extract the electron density, n_e, which is based on the fact that the X^- peak has a Lorentzian lineshape. We show that we can associate the numerator of the X^- Lorentzian lineshape to n_e. The method is described in details in the related papers. The determination of the electron density using optical spectrum has been discussed in several other works. In comparing our work to others we wish to note that the gated sample we used provided an independent measure for determining n_e, hence a check of the validity of our method can be performed. Our sample is basically a two-plate capacitor with the gate and the 2DES layers serving as the plates (see Fig. 9), hence, n_e should vary linearly with the gate voltage. In Fig. 13 I present the calculated n_e from our model. It is seen that it fits the linear line very well even when the X peak is negligible $\left(n_e > 3\cdot 10^{10} cm^{-2}\right)$. The obtained values are in good agreement with those measured by transport methods and the slope fits well to the geometrical capacitance of the sample.

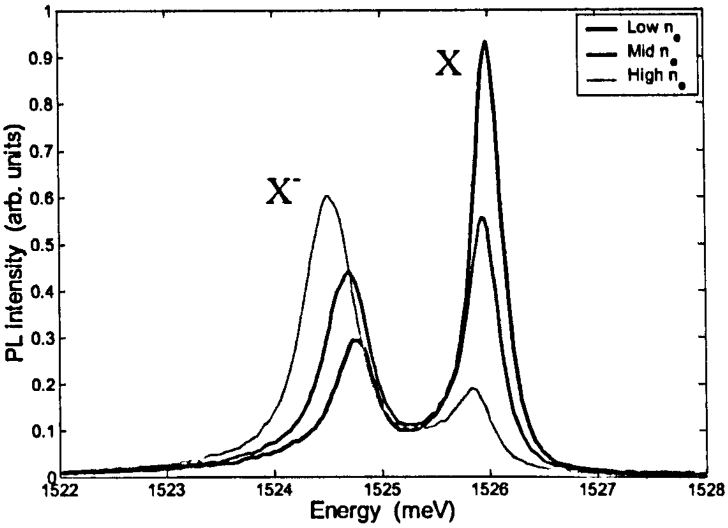

Fig. 11: PL spectra for three electron densities.

In References 41 and 42 the authors present a model for extracting n_e from the ratio between the X and X^- intensities, I_X and I_{X^-} respectively, assuming:

$$\frac{I_X}{I_{X^-}} = e^{(E_B-\mu)/K_BT}$$

where $\mu = K_BT\ln\left(e^{E_F/K_BT}-1\right)$ is the chemical potential, K_B is the Boltzman constant, T is the temperature, $E_F = \pi\hbar^2 n_e/m$ is the electron Fermi energy, and E_B is the X^- binding energy (see Fig. 12). To test this model they performed an experiment in which n_e was varied by changing the illumination intensity. The experimental results and the fit to that model are shown in Fig. 12. Unfortunately, the use of illumination to control the density does not allow an independent determination of n_e.

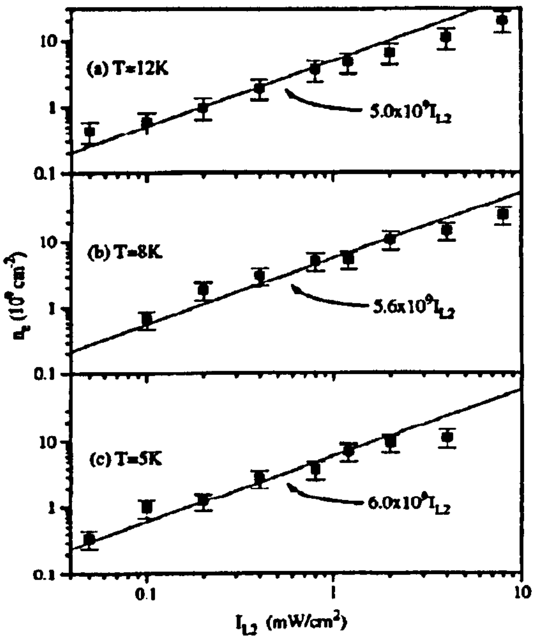

Fig. 12: Extracting n_e after Ref. [41].

We have tested this model by applying it to our data (Fig. 13). It is seen in the figure that the model of Ref. 41 gives a non-linear dependence of n_e on V_g. Furthermore, the obtained values of the electron density are higher than those measured by transport measurements and those known for the existence of the excitonic PL spectrum, which is typically smaller than $5 \cdot 10^{10} cm^{-2}$.

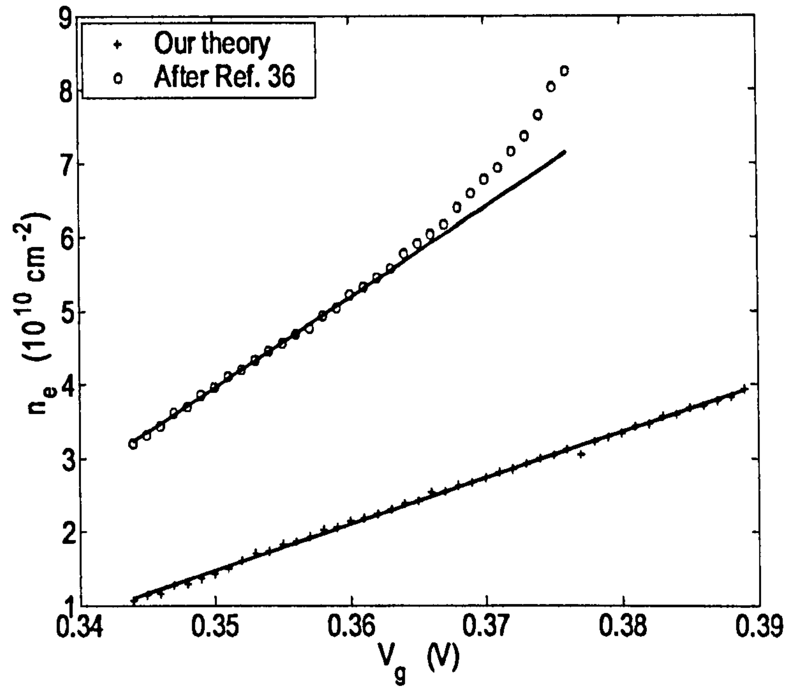

Fig. 13: Extracting n_e from the PL data by using our theory (+) and the theory of Ref. 41 (o). The solid lines are linear best fit for both models.

1.4.2 Broadening of the exciton lineshape.

Most previous local PL measurements where done on narrow QWs. In these systems the main broadening mechanism of the exciton line is well-width fluctuations [43]. In Fig. 14 it is seen how the wide far-field PL spectrum divides into many narrow peaks at different energies in the near-field spectrum. The narrow peaks are associated with localized excitons and they appear at different energies due to variations in the local well-width. We find that in high mobility 2DES samples with a wide QW this is not the main broadening mechanism for the X line.

We show that there is a clear correlation between the 2DEG density fluctuations and those of the X peak energies: regions with high (low) electron density give rise to a high (low) X peak energy. Hence, we conclude that the electron density fluctuations are the dominant broadening mechanism that determines the inhomogeneous width of the X peak. Thus, the far-field X width is a measure for the electron density fluctuations in the sample. This is a new broadening mechanism of excitons, and its contribution to the inhomogeneous X width in wide quantum wells is much larger than that of well-width fluctuations.

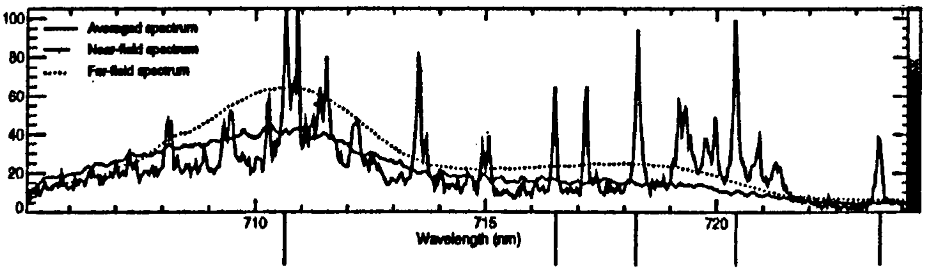

Fig. 14: Near-field and far-field spectra of 2.3 nm QW after H. F. Hess et al [43].

Related papers:

- Y. Yayon, M. Rappaport, V. Umansky and I. Bar-Joseph, "Excitonic emission in the presence of a two-dimensional electron gas: A microscopic view", Phys. Rev. B **64**, 081308 (2001).
- Y. Yayon, M. Rappaport, V. Umansky and I. Bar-Joseph, "The microscopic origin of the exciton-charged exciton spectrum", Physica Status Solidi (A) **190**, 607 (2002).

1.5 Correlations in the electron distribution and well width fluctuations in a quantum well

When dealing with disorder, an important question to ask is weather there is an underlying order. Are the fluctuations distributed randomly in the plane or are there any spatial correlations? In this work we addressed this question by performing high resolution spatial mapping of the QW properties and analyzing them.

One of the sources which might create long-range correlations in the QW properties is the well known phenomena of formation of mounds during the MBE growth. These mounds have a typical lateral extension of ~1 μm and height of ~10 nm for typical samples [44-46] (see Fig. 15).

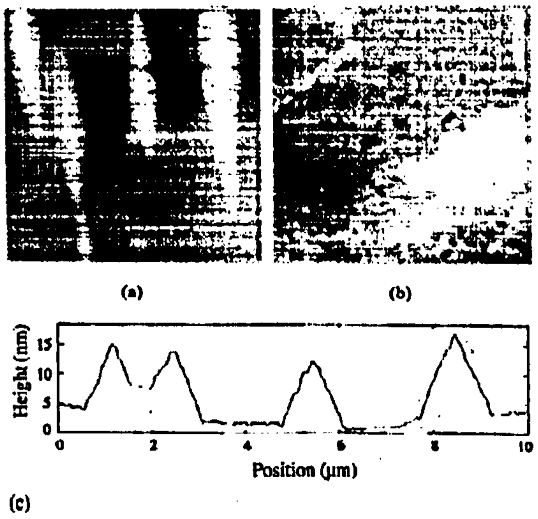

(a)10 μm×10 μm AFM scan of a 200 nm homoepitaxy GaAs surface after being annealed 30 min at 555 °C. The rms roughness over this area is 3.5 nm. The mounds are 10–15 nm high at their center points and have an aspect ratio of ~5 with a typical size of 6.6 μm×1.3 μm. They are elongated along the $[\bar{1}10]$ direction. (b) 2.3 μm×2.3 μm scan of the inset indicated in (a). The rms roughness over this area is 0.4 nm. The upper-half of the image is primarily one very large terrace. The cascading terraces on the lower-half of the image have an average width of 120 nm which corresponds to a slope of 0.1° (the nominal miscut). (c) A cross-sectional cut along the [110] direction. The slopes of the sides are ~1° all along the length of the mounds.

Fig. 15: After C. Orme et al. [45].

This mound formation process was recently reported even in the highest mobility samples that exist today ($\mu \sim 3\times10^7$ cm^2/V sec) [47,48]. In Fig. 16 (taken from Ref. 47) atomic force microscope (AFM) images of four high-mobility samples are presented. It is seen that in all samples anisotropic mounds exist and they are always elongated along the $[1\bar{1}0]$ crystallographic direction. The mounds height is up to 30 nm (more than 10 monolayers of GaAs).

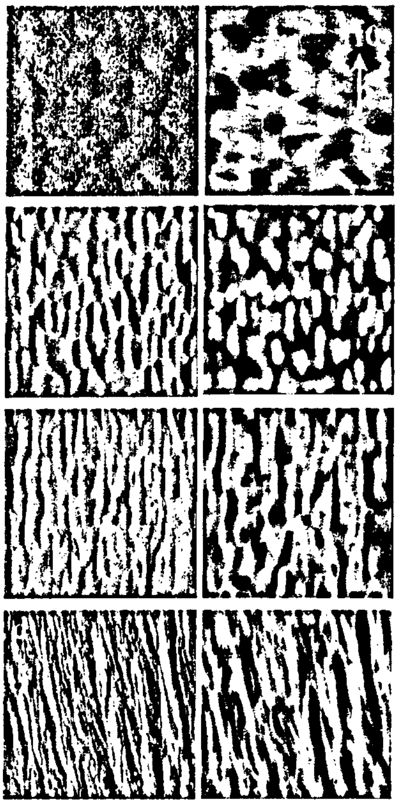

Fig. 16: After Willett et al. [47]. Representative range of surface morphologies of high-mobility heterostructures as measured with atomic force microscopy. Each field size is $20\mu m\times20\mu m$. The images on the right are surface topography, and the images on the left show variations in cantilever amplitude which are proportional to the topography derivative. Total vertical ranges for the topographic images are (a) 4 nm, (b) 10 nm, (c) 10 nm, (d) 30 nm.

For two-dimensional islands to turn into multilayered mounds more adatoms must land on top of them than hop off. Thus, the tendency to mound requires that the material exhibit a step edge barrier which impedes the motion of an adatom downward of a terrace (Fig. 17). Such a mechanism is provided by an intrinsic instability in the GaAs growth by MBE. It inhibits downward movement of adatoms at surface edges [44] due to the so-called Ehrlich-Schwoebel diffusion barriers at the edge of the terraces [33,34].

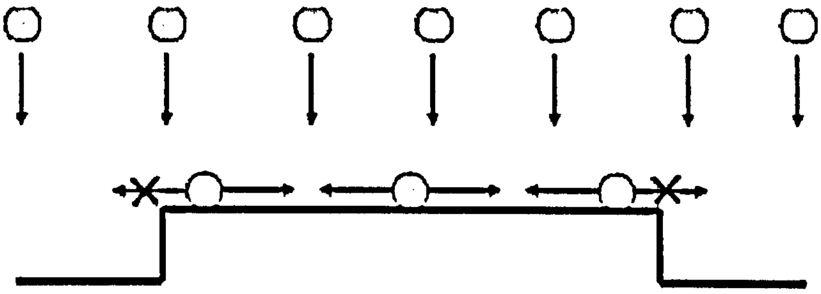

Fig. 17: Schematic visualization of the creation of traces due to the Enrlich-Schwoebel diffusion barriers.

The height of the mounds and their typical size increase with the number of layers grown in such a way that the inclination angle remains almost constant and equal to ~ 1°. As seen in Fig. 15 and Fig. 16 the mounds are usually in the form of ridges in the crystallographic direction $[\bar{1}10]$. This anisotropy in the mounds shape is due to the particular surface reconstruction of the last atomic layer that terminate the (001) surface. The dangling bonds of these atoms form dimmers that are arranged in rows and are the basic anisotropy which leads to the elongation of the mounds (see Fig. 18). The direction of the dimmer rows alternates each grown monolayer but usually GaAs growth is done at an As rich environment, where two monolayers are grown at once (a Ga monolayer and an As one immediately after) and the $[\bar{1}10]$ crystallographic direction is maintained.

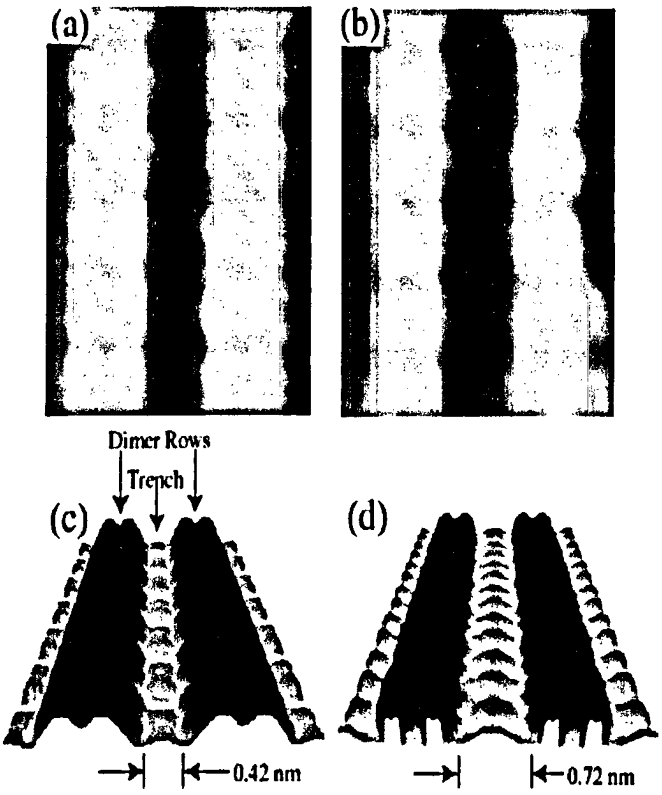

Fig. 18: STM image (a) and a model (c) of the reconstructed GaAs surface. After V. P. LaBella et al. [49].

This mound formation process produces variations in the width of any grown layer (for example: the QW layer, the spacer, and the distance between the surface and the QW). Let me demonstrate it by a simple model. In Fig. 19 (a) the growth of two layers is schematically shown. As I discussed earlier, the inclination angle of the mounds is kept constant during the growth, and the height and size of the mounds increase as more layers are grown. Notice the structural difference between the two layers: In layer 1 both interfaces consist of mounds which are separated one from the other, on the other hand in the upper interface of layer 2 the mounds are already connected. In Fig. 19 (b) the width of layer 1 ($\Delta L1$) and layer 2 ($\Delta L2$) are shown. The different behavior of the two layers is clearly seen: layer 1 is wider at the mounds and narrower at the trenches while layer 2 behaves in the opposite way. In our samples and also in Ref. [43], where the QW layer is grown after many layers (thickness of the order of 1 μm) and the mounds are already merged, the behavior is similar to that of layer 2 in the figure. Thus, the well is narrow at places where the surface is high and wide where it is low. This simple model does not explain all the growth properties. According to this model the mounds height decreases with the total layer growth, but experimentaly it is known that the behavior is the opposite.

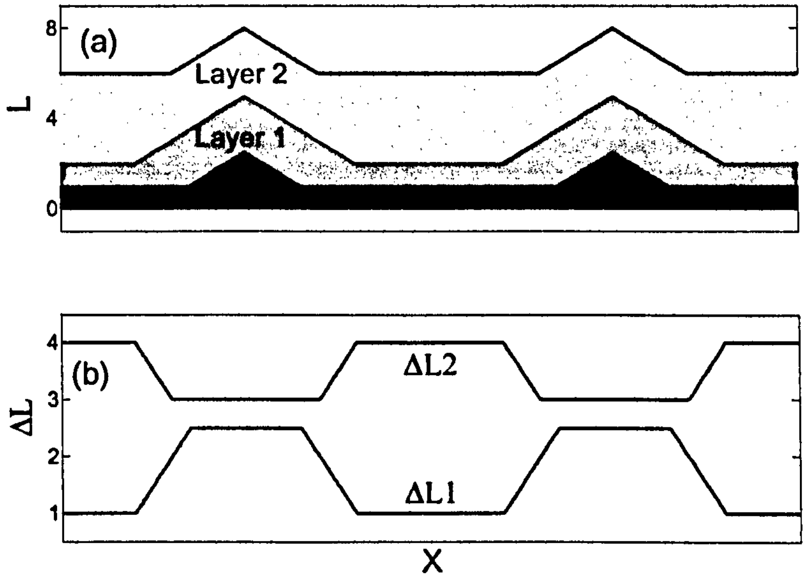

Fig. 19: (a) Schematic of the mounds formation. (b) Layers 1 and 2 width fluctuations.

Let me describe two main mechanisms where this growth process may influence the 2DES properties:

1.5.1 Well width fluctuations

As I showed before, the process of mounds formation during the MBE growth creates well width fluctuations. Let us see how it affects the properties of the charge carriers in a QW.

The quantization energy, E_n, of the charge carriers in a QW depends on the well width, L. For infinite well this relation is given by:

$$E_n = \frac{\hbar^2 n^2 \pi^2}{2mL^2},$$

where m is the charge carrier mass and $n = 1,2,\ldots$.

For finite well, E_n are given by the solution of the following equations:

$$k_w \tan\left(k_w \frac{L}{2}\right) = k_b \qquad \text{for even states}$$

$$k_w \operatorname{cotan}\left(k_w \frac{L}{2}\right) = -k_b \qquad \text{for odd states}$$

where $k_w = \sqrt{\frac{2m}{\hbar^2}(\varepsilon + V_b)}$, $k_b = \sqrt{-\frac{2m}{\hbar^2}\varepsilon}$, and V_b is the well depth. In Fig. 20 $\Delta E(\Delta L)$ for the exciton (E is taken as the sum of the electron and hole energies) is plotted for $L = 20$ nm for two cases: infinite well and finite barrier of Aluminum concentration of 0.37. It is seen that the amplitude of the energy fluctuations increases as the well width becomes narrower. Using this function we can associate measured exciton energy fluctuations with well width fluctuations as described in the related papers.

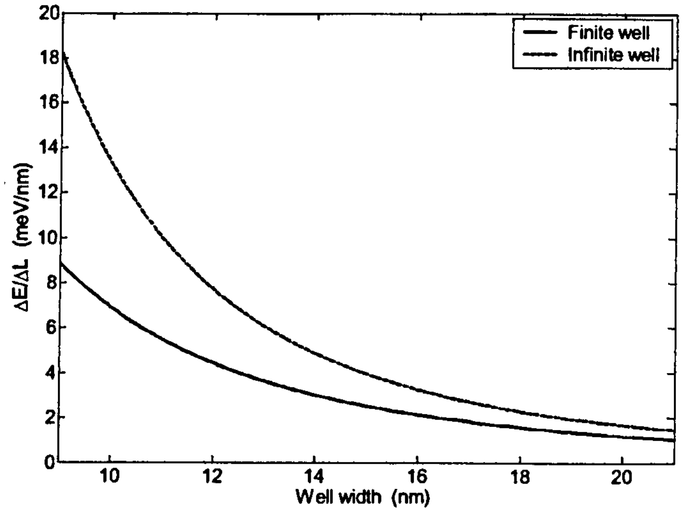

Fig. 20: $\Delta E/\Delta L(L)$ for finite and infinite quantum well.

1.5.2 Electrostatic potential fluctuations

When the distance between two charged layers fluctuates, potential fluctuations are created at both layers. For example if the distance between the 2DES layer and the surface changes then potential fluctuations are created in the QW which produce fluctuations in the electron distribution.

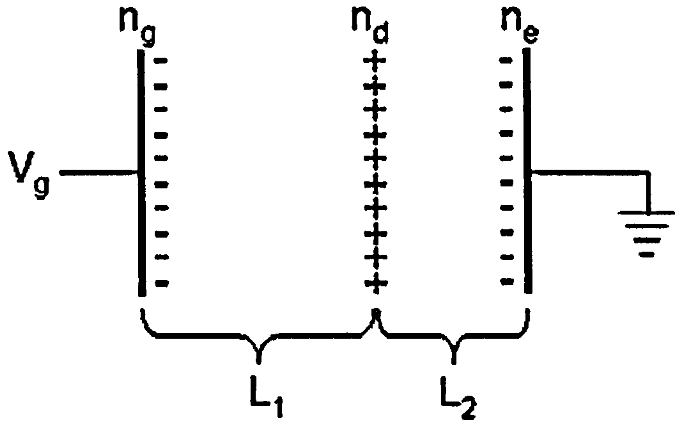

Fig. 21: A diagram of a gated 2DES structure.

Let me demonstrate it by a simple model. Assume a gated 2DES structure (see Fig. 21) with a gate voltage, V_g, applied between the gate and the QW. Between these two layers there is a donors layers of density, n_d. It is positioned at a distance of L_1 and L_2 from the surface and the QW, respectively. It can be easily shown, from electrostatic considerations, that the difference in electron density between the QW and the gate is given by:

$$n_e - n_g = \frac{2\varepsilon V_g}{eL} + \frac{(L-2L_2)}{L} n_d,$$

where ε is the material dielectric constant and $L = L_1 + L_2$ is the total distance between the surface and the QW. Let us assume a simple case where L remains constant but the spacer width (L_2) fluctuates. Then we derive from the above equation:

$$\Delta n_e = -\frac{\Delta L_2}{L} n_d ,$$

where from charge conservation I assumed $\Delta n_e = -\Delta n_g$. Let us take typical values of $L = 100$ nm, $n_d = 10^{12}$ cm^{-2}, and $\Delta L_2 = 0.28$ nm (one monolayer of GaAs). We get that a small fluctuation in the spacer width leads to a significant electron density change in the QW of $\Delta n_e = 2.8 \cdot 10^9$ cm^{-2}.

We performed simultaneous local measurements of the surface topography, well width, and electron density. We found that the electron density distribution and well width fluctuations are strongly affected by the mounds formation and that there is a surprising order in the distribution of these quantities.

Related papers:

- Y. Yayon, M. Rappaport, V. Umansky and I. Bar-Joseph, "Anisotropy and periodicity in the density distribution of electrons in a quantum well", Phys. Rev. B 66, 033310 (2002).
- Y. Yayon, A. Esser, M. Rappaport, V. Umansky, H. Shtrikman and I. Bar-Joseph, "Near-field spectroscopy of well-width and electron density fluctuations in GaAs/AlGaAs quantum well", Proceeding of ICPS26, Edinburgh, Scotland (2002).
- Y. Yayon, A. Esser, M. Rappaport, V. Umansky, H. Shtrikman and I. Bar-Joseph, "Long-range spatial correlations in the exciton energy distribution in GaAs/AlGaAs quantum-well", Phys. Rev. Lett. 89, 157402 (2002).

2 Main results

2.1 Published papers

The main part of my work is published in the following papers:

- G. Eytan, Y. Yayon, I. Bar-Joseph, and M. L. Rappaport, "A storage Dewar near-field scanning optical microscope", Ultramicroscopy, **83**, 25 (2000).
- Y. Yayon, M. Rappaport, V. Umansky and I. Bar-Joseph, "Excitonic emission in the presence of a two-dimensional electron gas: A microscopic view", Phys. Rev. B **64**, 081308 (2001).
- Y. Yayon, M. Rappaport, V. Umansky and I. Bar-Joseph, "The microscopic origin of the exciton-charged exciton spectrum", Physica Status Solidi (A) **190**, 607 (2002).
- Y. Yayon, M. Rappaport, V. Umansky and I. Bar-Joseph, "Anisotropy and periodicity in the density distribution of electrons in a quantum well", Phys. Rev. B **66**, 033310 (2002).
- Y. Yayon, A. Esser, M. Rappaport, V. Umansky, H. Shtrikman and I. Bar-Joseph, "Near-field spectroscopy of well-width and electron density fluctuations in GaAs/AlGaAs quantum well", Proceeding of ICPS26, Edinburgh, Scotland (2002).
- Y. Yayon, A. Esser, M. Rappaport, V. Umansky, H. Shtrikman and I. Bar-Joseph, "Long-range spatial correlations in the exciton energy distribution in GaAs/AlGaAs quantum-well", Phys. Rev. Lett. **89**, 157402 (2002).

2.2 Unpublished results

2.2.1 Spatial distribution of impurities in a quantum well

In the following paragraph I'll describe part of my work which was not published in the form of a paper.

All intrinsic GaAs samples are not ideally pure and they always contain some density of impurities which can behave as acceptors or donors. In our samples this background doping is mainly acceptors and has a typical density of $\sim 10^{14} - 10^{15} cm^{-3}$. A massive theoretical [50-53] and experimental [54-57] work was done in the past two decades to characterize the properties of these impurities.

In this work I present a method for simultaneously measuring the local distribution and the binding energy of acceptors in a QW. We measured the PL spectrum from an ungated sample at a magnetic field applied perpendicular to the 2DES layer. The spectrum exhibits peaks, which correspond to the different Landau levels. We found that at some spatial points there is a duplication of the 2DES spectrum at a lower energy (see Fig. 22).

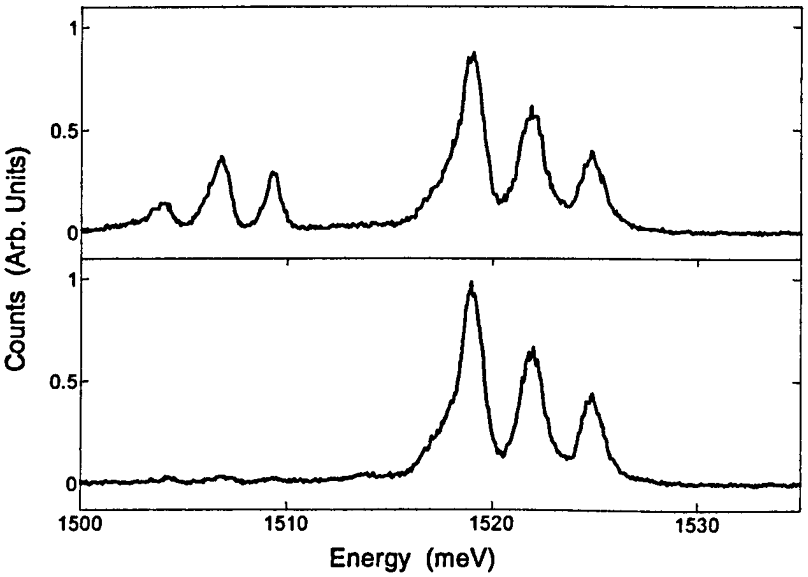

Fig. 22: Two PL spectra at different points of the sample which are 0.5 μm apart. Note the additional low energy peaks at the top spectrum.

The fact that the spectrum is duplicated and shifted to lower energies allows us to identify it as a recombination of an electron from the 2DES with a hole bound to a native acceptor in the quantum well. The red shift of the spectrum is the binding energy of the hole to the acceptor. Thus, we have a method to map the acceptors binding energy and spatial location.

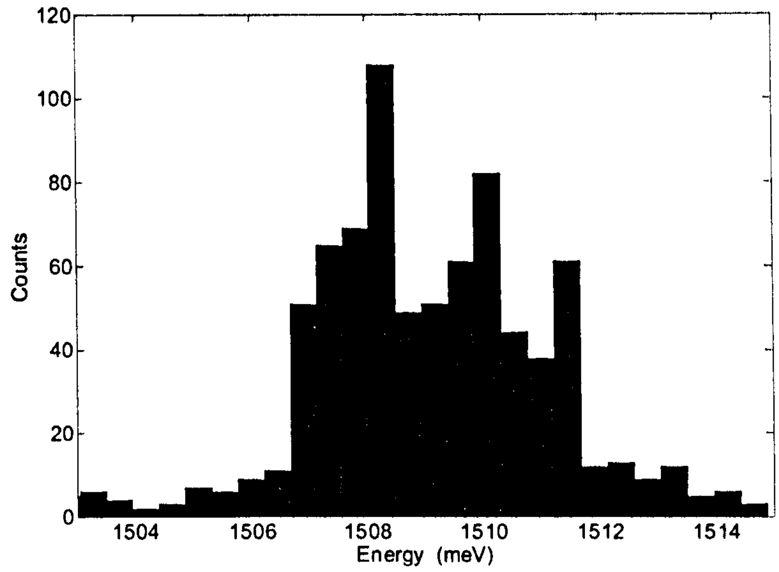

Fig. 23: Histogram of the acceptor energies.

To find the local binding energy of the acceptors we need to calculate at each point the red shift in energy of the duplicated spectrum from the main spectrum. This is done by calculating the difference in the energy center of mass of the two spectra. In Fig. 23 the energy center of mass of the acceptor spectrum (low energy duplication of the spectrum) is presented as a histogram. The free-hole spectrum is centered around ~1523 meV, thus the acceptor binding energies are distributed between 11 and 16 meV. The binding energy of a hole to an acceptor in bulk GaAs is constant (~30 meV) [56] and is higher than that obtained in our measurement. The smaller binding energies and their wide distribution can be explained if we assume that the acceptors are located close to the quantum well edge. Theoretical calculations of such acceptors show a spread of binding energies in a range similar to our observation [55].

In Fig. 24 we present a grayscale color map of the integrated intensity of the low energy part of the spectrum, which reflects the acceptor spatial distribution. The acceptors two-dimensional density that we measure is ~10^8 cm^{-2}, which is in a good agreement with typical values for the background doping in MBE grown GaAs wafers.

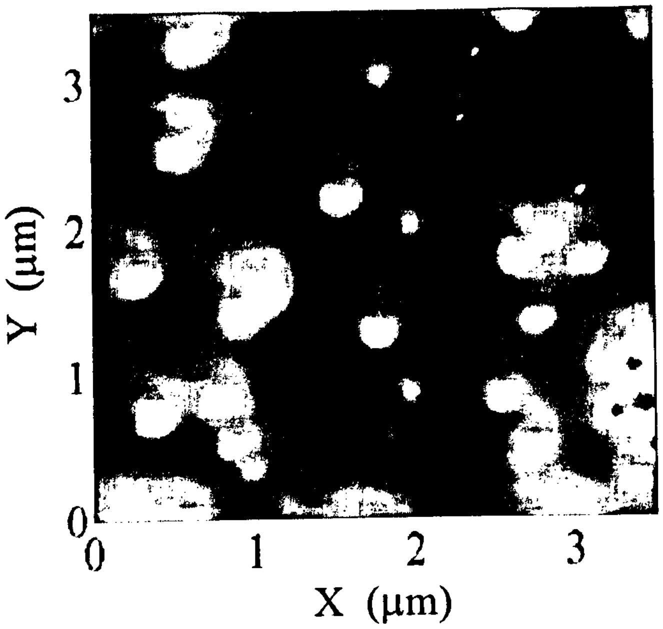

Fig. 24: Acceptor distribution. Bright points represent high density.

3 Summary

In this work I studied the disorder of a 2DES in a GaAs QW using near-field optical spectroscopy.

3.1 Instrumentation

We designed and built a SNOM for operation within a storage Dewar at a temperature of 4.2 K. It was designed for studies of opaque samples and operates in the collection mode. Its rigidity allows high resolution and long scans with no additional vibration isolation. Its compact design allows it to be inserted into a superconductor magnet and we have tested it in a high magnetic field of up to 9 T. I used the tube etching method to fabricate optical fiber tips with high resolution (100-300 nm) and high transmission ($>10^{-3}$).

3.2 Excitonic spectrum in the presence of a two-dimensional electron system

I performed near- and far- field photoluminescence (PL) measurements of a gated two-dimensional electron system (2DES) for understanding the microscopic origin of the different lineshapes of the neutral (X) and negatively charged exciton (X^-). I found a new broadening mechanism of the X line: local density fluctuations give rise to spatial fluctuations of the local X peak energy, and hence to inhomogeneous broadening of the far-field X line. On the other hand, I found that the X^- is homogeneously broadened, and the numerator of its Lorentzian lineshape is linearly proportional to the electron density in the QW. I present a novel method to determine the electron density from the PL spectrum.

3.3 Correlations in the electron distribution and well width fluctuations in a quantum well

The variations in the well-width and in the electron density in the plane of a QW are measured by near-field spectroscopy. I exploit the local PL spectrum to construct two-dimensional images of the electron density and well width fluctuations. By analyzing the correlation function of these images I find that there is profound long-range order in the electron distribution and well width fluctuations. We found that the electrons in the QW are arranged in stripes of elongated parallel to the $[1\bar{1}0]$ crystallographic direction. The width of the stripes is smaller than 150 nm and their period is of the order of ~ 1 μm. We have shown that the well width fluctuations form a periodic structure which resembles a cubic lattice with a period larger than 1 μm. Strong long range correlations appearing laterally, in the plane of the QW, as well as vertically, between QWs grown one on top of the other. I show that these fluctuations are correlated with the commonly found mound structure on the surface.

3.4 Spatial distribution of impurities in a quantum well

I performed near-field PL measurements of a 2DES in a perpendicular magnetic field. At some specific locations in the sample the known spectrum of a 2DES in a magnetic field is duplicated at a lower energy. This low energy spectrum is identified as a recombination of a free electron from the QW with a hole bound to an acceptor. We use the low-energy spectrum to obtain the binding energy and location of the acceptors in a QW. We found that the acceptor binding energies are distributed between 11 and 16 meV and their density is $\sim 10^8$ cm^{-2}.

4 References

---

1. D. W. Pohl, W. Denk, and M. Lanz, Appl. Phys. Lett. **44**, 651 (1984).
2. G. Binning, H. Rohrer, Ch. Gerber, and E. Weibel, Surface studies by scanning tunneling microscopy, Phys. Rev. Lett. **49**, 57 (1982).
3. G. Binning, C. F. Quate, and Ch. Gerber, Atomic force microscope, Phys. Rev. Lett. **56**, 930 (1986).
4. M.A. Paesler, P.J. Moyer, "Near-field optics" (Wiley-interscience press, New York, 1996), Chap 4.
5. M. Born, and E. Wolf, "Principles of optics" (Pergamon press, London, 1965).
6. G.A. Massey, Appl. Opt. **23**, 658 (1984).
7. J.M. Vigoureux, and D. Courjon, Appl. Opt. **31**, 3170 (1992).
8. J.M. Vigoureux, F. Depasse, and C. Girard, Appl. Opt. **31**, 3036 (1992).
9. E. Betzig, P. L. Finn, and J. S. Weiner, Appl. Phys. Lett. **60**, 2484 (1992).
10. R. D. Grober, T. D. Harris, J. K. Trautman, and E. Betzig, Rev. Sci. Instrum. **65**, 626 (1994).
11. A. Drabenstedt, J. Wrachtrup, and C. von Borczyskowski, Appl. Phys. Lett. **68** (24), 3497 (1996).
12. J. Barenz, O. Hollricher, and O. Marti, Rev. Sci. Instrum. **67** (5), 1912 (1996).
13. Y. Chuang, C. wang, J. Y. Huang, and C. Pan, Appl. Phys. Lett. **69** (22), 3312 (1996).
14. Walid A. Atia and Christopher C. Davis, Appl. Phys. Lett. **70** (4), 405 (1997).
15. Khaled Karrai and Robert D. Grober, Appl. Phys. Lett. **66**, 1842 (1995).
16. K. T. Flaming and D. G. Brown, "Advanced Micropipette Techniques for Cell Physiology" (Wiley Interscince, Chichester, 1986).
17. E. Betzig and J. K. Trautman. Scinece **257**, 189 (1992).
18. M. garcia-Parajo, E. Cambril ,and Y. Chen, Appl. Phys. Lett. **65**, 1498 (1994).
19. W. P. Ambrose, P. M. Goodwin, J. C. Martin, and R. A. Keller, Science **265**, 364 (1994).
20. B. I. Yacobson, P. J. Moyer, and M. A. Paesler, J. Appl. Phys. **73**, 7984 (1993).
21. H. Bielefeldt et al, Appl. Phys. A **59**, 103 (1994).

22. E. Betzig et al, Appl. Phys. Lett. **63**, 3550 (1993).
23. G. A. Valaskovic, M. Holton, and G. H. Morrison, Appl. Opt. **34**, 1215 (1995).
24. B. Schoch, B. E. Jones and A. Franks, Meas. Sci. Tech. **5**, 663 (1994).
25. P. Hoffmann, B. Dutoit, and R. P. Salathe, Ultramicroscopy **61**, 165 (1995).
26. D. Courjon, C. Bainier, and M. Spajer, J. Vac. Sci. Technol. B **10**, 2436 (1992).
27. S. I. Bozhevolnyi, O. Keller, and I. I. Smolyaninov, Opt. Lett. **19**, 1601 (1994).
28. S. I. Bozhevolnyi, M. Xiao, and O. Keller, Appl. Opt. **33**, 876 (1994).
29. S. I. Bozhevolnyi, O. Keller, and M. Xiao, Appl. Opt. **32**, 4864 (1993).
30. R.C. Reddick et al, Rev. Sci. Instr. **61**, 3669 (1990).
31 P. Lambelet, A. Sayah, M. Pfeffer, C. Philipona, and F. Marquis-Weible, Appl. Opt. **37**, 7289 (1998).
32. R. Stockle, C. Fokas, V. Deckert, R. Zenobi, B. Sick, B. Hecht, and U. Wild, Appl. Phys. Lett. **75**, 160 (1999).
33. G. Ehrlich et al., Chem. Phys. **44**, 1039 (1996).
34. .L. Schwoebel et al., J. Appl. Phys. **37**, 3682 (1996).
35. A. L. Efros, Solid State Commun. **65**, 1281 (1988).
36. A. L. Efros, Solid State Commun. **70**, 253 (1989).
37. A. L. Efros et al., Phys. Rev. B **47**, 2233 (1993).
38. K.Kheng *et al.*,Phys.Rev.Lett. **71**, 1752 (1993).
39. G. Finkelstein, H. Shtrikman, and I. Bar-Joseph, Phys. Rev. Lett. **74**, 976 (1995).
40. A. J. Shields *et al.*, Phys. Rev. B **51** ,18049 (1995).
41. A. Menassen et al., Phys. Rev. B **54**, 10609 (1996).
42. A. Ron *et al.*, Solid State Commun. **97**, 741 (1996).
43. H. F. Hess et al., Science **264**, 1740 (1994).
44. M. D. Johnson *et al.*, Phys. Rev. Lett. **72**, 116 (1994).
45. C. Orme *et al.*, Appl. Phys. Lett. **64**, 860 (1994).
46. G. Apostolopoulos et al., Phys. Rev. Lett. **84**, 3358 (2000).
47. R.L. Willett et al., Phys. Rev. Lett. **87**, 126803-1 (2001).
48. K.B. Cooper et al., Solid State Commun. **119**, 89 (2001).
49. V. P. LaBella et al., http://www.uark.edu/misc/mbestm/gaas2x4/gaas2x4_info.html

---

50. J. Menchero, and T. Boykin, Phys. Rev. B **59**, 8137 (1999).

51. V. Fiorentini, Phys. Rev. B **51**, 10161 (1995).

52. L. Oliveira, and J. Lopez-Gondar, Phys. Rev. B **41**, 3719 (1990).

53. A. Pasquarello, et al., Phys. Rev. B **40**, 5602 (1989).

54. L. Bryja, M. Kubisa, K. Ryczko, et al., Solid State Commun. **122**, 379 (2002).

55. G. Rune, et al., Phys. Rev. B 44, 4010 (1991).

56. L. Greene, and K. Bajaj, Solid State Commun. **53**, 1103 (1985).

57. V. Swaminathan, et al., J. of Appl. Phys. **53**, 5163 (1982).